Atomic-Scale Mechanisms of Electrochemical Pt Dissolution

Zhiyao Duan* and Graeme Henkelman*

ACCESS | Metrics & More | Article Recommendations | Supporting Information

ABSTRACT: Pt dissolution under potential cycling has been identified as the dominant process that causes cathode losses in proton-exchange membrane fuel cells. In recent years, significant insights on the Pt dissolution process have been obtained from in situ Pt dissolution detection enabled by voltammetry coupled to inductively coupled plasma mass spectrometry. Despite extensive experimental research, theoretical studies continue to lag in the understanding of the atomic-scale mechanism of the Pt dissolution process due to the complicated subprocesses involved, including Pt oxidation, surface reconstruction, Pt oxide reduction, chemical corrosion, etc. Here, we employ global optimization and constant-potential density functional theory to simulate the complete process of Pt dissolution. We show that a two-dimensional Pt surface oxide consisting of interconnected square planar PtO_4 units forms at applied potentials higher than 1.1 V_{RHE}. The structural signatures and oxidation states of the Pt surface oxide are close to that of bulk Pt_3O_4 oxide. The PtO_4 units can be reduced to $[PtOH(H_2O)_3]^+$ in the cathodic scan and dissolve into the electrolyte. The dissolved $[PtOH(H_2O)_3]^+$ species favorably accepts a proton and becomes $[Pt(H_2O)_4]^{2+}$. We also find that the dissolution of one Pt atom leads to the decomposition of the connected $Pt(OH)_4$ units because of ligand losses, which then renders them susceptible to be reduced to Pt^0. On the basis of our findings, we propose a cathodic Pt dissolution mechanism: $Pt_3O_4^s + 8H^+ + 6e^- \rightarrow [Pt(H_2O)_4]^{2+} + 2Pt$. An anodic Pt dissolution mechanism is also proposed. Our work provides a fundamental understanding of Pt dissolution under potential cycling, which is needed for the rational design of durable Pt-based cathodes for fuel cells.

KEYWORDS: density functional theory, constant-potential calculations, Pt dissolution, oxygen reduction reaction, Pt oxidation, potential cycling
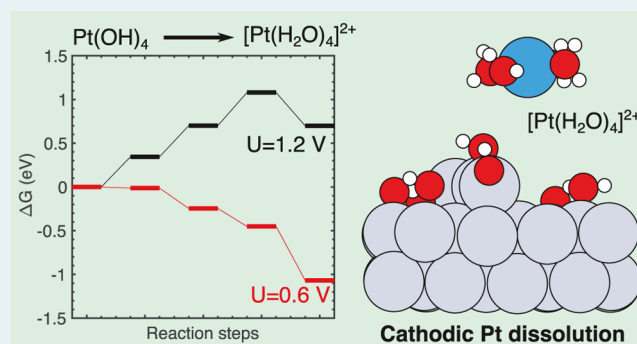
INTRODUCTION

The consumption of fossil fuels by the industrial activities of human beings over the last 300 years has induced severe environmental hazards and climate change. The utilization of clean energy sources, which can greatly reduce carbon emissions, is still a great challenge facing our society. Proton-exchange membrane fuel cells (PEMFCs) can directly convert hydrogen fuel into electrical power at low temperature, which makes them attractive for replacing fossil-fuel-based combustion engines in vehicles. The efficiency and durability of Pt-based electrocatalysts catalyzing the oxygen reduction reaction (ORR) in the cathode of PEMFCs are two limiting factors that need to be overcome before fuel cell cars can be accepted by the mass market.[1] To assist the directed development of efficient and durable Pt-based ORR catalysts, key fundamental descriptors that govern both the activity and stability trends are needed.

Theoretical guidelines on how to improve the activity of ORR electrocatalysts have emerged on the basis of a fundamental understanding of the ORR reaction mechanism and surface adsorption properties of electrocatalysts.[2] Regarding the degradation of Pt-based ORR electrocatalysts, Pt dissolution has been identified as the dominant process causing the observed loss of the active surface area under operating conditions of fuel cells.[3,4] However, detailed atomic-scale mechanism of Pt dissolution has not been fully understand, which hinders further development of Pt dissolution mitigation strategies. In the literature, to the best of our knowledge, first-principles simulations of the complete Pt dissolution process have not been conducted. There have been several theoretical studies focused on Pt surface oxidation and subsequent Pt extraction.[5−8] The atomic-level mechanism of the actual dissolution of Pt, however, still remains uncertain.

Experimentally, by coupling voltammetry with inductively coupled plasma mass spectrometry (ICP-MS), the real-time detection of potential-dependent Pt dissolution has been enabled and significant insights into the Pt dissolution process have been achieved.[9−15] In potential cycling experiments, which
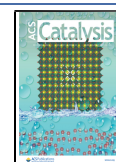
mimic the start/stop cycles of a PEMFC-powered automotive, it was observed that Pt dissolution occurs only when the upper limit of the applied potential profile exceeds 1.1 V_{RHE} and the amount of dissolved Pt increases with an increasing upper potential limit.[9] More importantly, the majority of Pt dissolution was found to occur during the negative-going potential scan, which is denoted as cathodic dissolution.[9] Anodic Pt dissolution (Pt dissolution during the positive-going potential scan) was also observed, but found to be minor as compared to cathodic dissolution.[9,14] These findings suggest that the majority of Pt dissolution is related to Pt oxide formation in the anodic scan and the subsequent reduction of Pt oxide in the cathodic scan.

Herein, we present a density functional theory (DFT) study on the full reaction path of the Pt dissolution process on the Pt(111) surface during potential cycling. We focus primarily on the cathodic Pt dissolution process, which involves Pt surface oxidation, Pt oxide reduction, and Pt detachment as subprocesses. To this end, we employed a global optimization method to obtain realistic structures of Pt surface oxides formed during the anodic scan. In addition, DFT calculations under constant-potential conditions are used to investigate the reduction of the surface oxide in the cathodic scan. The advantage of the constant-potential method is that it can decouple the introduction of H^+ and e^-, which allows to distinguish between an electrochemical reduction reaction and a chemical H^+ addition reaction. Our study provides insights on the atomic-scale mechanism of the Pt dissolution process under potential cycling along with potential-dependent energetic information of the process. The fundamental understanding of the Pt dissolution process obtained in this study can facilitate the directed design of durable Pt-based ORR electrocatalysts.

■ COMPUTATIONAL METHODS

DFT calculations with a plane-wave basis set were performed using the Vienna ab initio simulation package.[16−18] Electronic exchange and correlation were described using the Perdew−Burke−Ernzerhof (PBE) functional.[19] Electron−ion interactions were described within the projector augmented wave framework.[20] In all calculations, the energy cutoff of the plane-wave basis set was 400 eV.

Slab models consisting of five Pt layers with 16 atoms in each layer were employed to model the Pt(111) surface. The bottom two layers were fixed during structural relaxation. A 20 Å vacuum gap was used to eliminate interactions between periodic images perpendicular to the slab surface. The Brillouin zone integration in k-space was performed on a $4 \times 4 \times 1$ k-point mesh sampled using the Monkhorst−Pack scheme.[21] Optimized structures were obtained by minimizing the forces on each ion until they fell below 0.05 eV/Å. A Bader charge analysis was carried out using software developed by the Henkelman group.[22,23]

We employed the genetic algorithm implemented in the atomic simulation environment to perform global optimization of structures of Pt surface oxides.[24] We generated 20 different structures by randomly placing 16 Pt atoms and various number of O atoms above the Pt slab as the initial population for the genetic algorithm searches. The initial structures were then subjected to pairing and mutation operations to evolve the population until the search converged to a low energy minimum.

Constant-potential calculations were performed by making a generalized force via expanding the force of the system with the negative value of the electrochemical potential of electrons $\overline{\mu}_e$ so that the coordinates and the number of electrons of the system

could be optimized simultaneously according to the target applied potential on the SHE scale, i.e., U_{SHE}. $\overline{\mu}_e$ is calculated as

$$\overline{\mu}_e = \mu_{e,SHE} + eU_{SHE} \qquad (1)$$

where $\mu_{e,\,SHE}$ is the electronic chemical potential of the system referring to the SHE

$$\mu_{e,SHE} = E_f - e(V_{sol} - \Phi_{SHE}/e) \qquad (2)$$

in which E_f is the Fermi level, V_{sol} is the potential deep in the solution, and Φ_{SHE} is the work function of the SHE. Here, we take Φ_{SHE} to be −4.6 eV. Hence, the grand canonical energy of the system is calculated as

$$\Omega = E_{DFT} + \Delta n \cdot (U_{SHE} - V_{sol} + \Phi_{SHE}/e) \qquad (3)$$

In this equation, E_{DFT} is the energy calculated from DFT and Δn is the number of electrons added or removed from the system. Thus, the electrochemical potential of electrons $\overline{\mu}_e$ is calculated as

$$\overline{\mu}_e = \frac{\partial \Omega}{\partial n} = (E_f - V_{sol} + \Phi_{SHE}/e) + U_{SHE} \qquad (4)$$

By setting Ω and $\overline{\mu}_e$, the structures were optimized under constant-potential conditions. In the constant-potential calculations, we employed VASPsol for the implicit solvation model. For our charged systems, a counter-ion charge distribution is included in the implicit solvent region through the use of the generalized Poisson−Boltzmann equation. We used a Debye length of 3 Å to mimic the experimental condition where 1 M of a strong acid is used. The dielectric constant of the electrolyte was set to 80. It should be noted that the short Debye length allows the counter charge to stay close to the electrode surface and results in a flat electrostatic potential in the center of the solution region due to the screening effect of the electrolyte. Thus, symmetric slab structures are not needed to calculate V_{sol}.[25] This constant-potential method has recently been applied to calculate electrochemical reaction barriers; the code for these calculations is freely available.[26]

In calculations of the reaction free energies, we included free-energy corrections for the free reaction species. Specifically, the TS for H^+ and H_2O in bulk solution are 0.205 and 0.67 eV, respectively.[2] The entropy of free dissolved species is also calculated. We estimate the translational and rotational entropy (S_{trans} and S_{rot}) using the simple ideal gas model. The $T(S_{trans} + S_{rot})$ of $[Pt(OH)(H_2O)_3]^+$ and $[Pt(H_2O)_4]^{2+}$ is calculated to be 0.9 eV at standard conditions. The vibrational entropy for the dissolved species is ignored because we assume that the contribution is similar before and after dissolution. The entropies of adsorbed species are also neglected.

■ RESULTS AND DISCUSSION

Electrochemical Oxidation of Pt(111). We performed global optimizations using a genetic algorithm to obtain stable structures of Pt surface oxides of various O coverages over the Pt(111) surface. The studied O coverages range from 1/4 monolayer (ML) to 1 ML in increments of 1/8 ML. The energy convergence with respect to the optimization steps is shown in Figure S1. The optimized structures and their corresponding energies are used to construct the surface Pourbaix diagram as shown in Figure 1. In addition to the clean Pt(111) surface, there are five Pt surface oxide phases, namely, the Pt(111) surface with 1/4, 3/8, 1/2, 3/4, and 1 ML O, which are thermodynamically stable under the electrochemical conditions relevant for ORR.
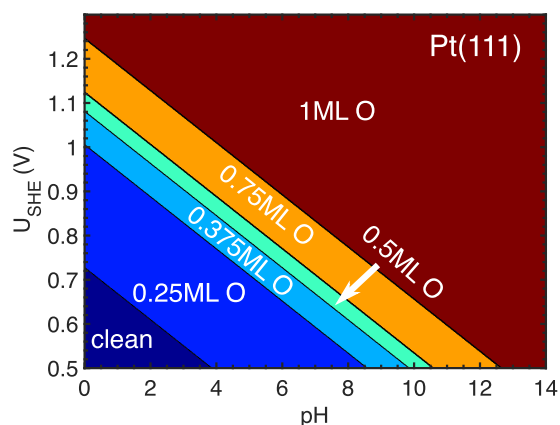
Figure 1. Surface Pourbaix diagram of Pt surface oxides on Pt(111) found by global optimization.

The surface structures of these stable surface phases on the surface Pourbaix diagram are shown in Figure 2. The surface phases not shown in the surface Pourbaix diagram are shown in Figure S2. In Figure 2, histograms of the Pt−O coordination number (CN) counts and the oxidation-state distributions of the surface Pt atoms in various surface phases are also shown. The Bader charges of the surface Pt atoms are used for the oxidation-state analysis. To convert Bader charges to formal oxidation states, we use the Bader charges of Pt atoms in Pt bulk oxides, namely, PtO, Pt_3O_4, and PtO_2, as references for Pt^{2+}, $Pt^{2.7+}$, and Pt^{4+}, respectively. For O coverages from 1/4 to 1/2 ML, as can be seen in Figure 2a−c, the O atoms are adsorbed at 3-fold hollow sites. The surface Pt atoms coordinate with one−two O atoms and are only mildly displaced from their original lattice sites upon O adsorption, so the surfaces remain smooth at these relatively low O coverages. The oxidation states of the surface Pt atoms are in between Pt^0 and Pt^{2+}, indicating that surface Pt atoms are in the surface adsorption states. The 1/4 ML O surface phase starts to form when the electrode potential is above 0.7 V_{RHE}, and as the potential goes up, the O coverage eventually increases to 3/8 and 1/2 ML when the potential reaches 1.0 and 1.1 V_{RHE}, respectively. At these low O coverages, our results are similar to previous results showing that the onset potentials for 1/4, 1/3, and 1/4 ML O phases are approximately 0.8, 1.0, and 1.1 V, respectively.[27]

Beyond 1/2 ML O, the surface structure undergoes significant reconstructions. For the 3/4 ML O state, as shown in Figure 2d, corner-sharing square planar PtO_4 units formed on the surface. The 3/4 ML O phase is stable under electrode potentials ranging from 1.12 to 1.24 V_{RHE}. These PtO_4 units sit above the original Pt(111) surface layer by 2.2 Å, on average. The oxidation states of these PtO_4 units are similar to that of the Pt_3O_4 oxide ($Pt^{2.7+}$), which indicates a phase transformation from the surface adsorption state to a surface Pt oxide. The height of the PtO_4 unit is close to that observed by surface X-ray diffraction (SXRD), which showed that surface Pt atoms lie 2.4 Å above their original lattice after oxidation at $U = 1.17$ V.[28,29] Experiments have attributed Pt buckling to a place exchange process in which the original lattice sites of surface Pt atoms were taken by O atoms.[28,29] Our simulation, however, shows a different picture, where O atoms have not penetrated into the Pt lattice sites at this stage but rather mainly lie above the original Pt surface in the form of Pt surface oxide. This is in line with the 2D surface nucleation and growth mechanism proposed by Gómez-Marín and Feliu et al.[30,31] The fraction of surface Pt

atoms being oxidized to form surface oxide is 0.25 (4 out of the 16 Pt atoms), which is also consistent with the SXRD study showing 22% so-called place-exchanged Pt atoms at $U = 1.17$ V.[28]

In the 1 ML O phase, the surface further reconstructs and becomes disordered and rough. We see the formation of PtO_3, PtO_4, and even PtO_5 oxide units on the surface, as can be seen in Figure 2e. Here, O penetration has occurred and the oxidation straddles two atomic layers with a thickness of about 4.5 Å. The 1 ML O surface phase is stable above the electrode potential of 1.24 V_{RHE}. These computational results are consistent with the experimentally observed 5 Å thick disordered Pt oxide layer at $U = 1.57$ V.[28] A recent theoretical study found a surface PtO phase consisting of stripes of edge-shared PtO_4 units with an onset potential of 1.3 V on the surface Pourbaix diagram.[32] Our high O-coverage phases have lower onset potentials than that of the surface PtO phase, which adds support to the reasonableness of our surface Pourbaix diagram constructed from our globally minimized structures. However, it should be noted that the experimental conditions in aqueous models do not fully represent the gas diffusion electrode employed in the real PEMFC device.[33] In addition, the Nafion membrane on the catalyst layer can also influence the behavior of Pt oxidation or Pt dissolution.[33]

Electrochemical Reduction of Pt Surface Oxide and Pt Dissolution. Experimentally, Pt starts to dissolve considerably only when the positive-going potential limit exceeds 1.15 V_{RHE} during potential cycling.[9] The 3/4 ML O surface phase is the thermodynamically stable phase at 1.15 V_{RHE}. The surface phase is characteristic of the 2D Pt surface oxide consisting of interconnected PtO_4 units. The structural signatures of the 2D Pt surface oxides resemble the structure of bulk Pt_3O_4 oxide (see Figure S3). The oxidation state of the Pt surface oxide is also close to that of Pt_3O_4. In situ X-ray adsorption fine structure (XAFS) measurements demonstrated that the direct transformation from Pt^0 into mostly Pt^{2+} at the nanoparticle surfaces occurs at potentials above 1.2 V, and no further oxidation to Pt^{4+} was observed under fuel cell operating conditions.[34] In situ X-ray photoelectron spectroscopy (XPS) studies also confirm that the oxidized Pt appearing at voltages >1.0 V was ascribed to Pt^{2+}.[35] The formation of bulk PtO_2 after prolonged application of a high positive voltage has been reported, but such conditions are essentially different from the the operating conditions of PEMFCs.[36,37] Overall, the 3/4 ML O surface phase is a good match with experimental results of structural and electronic characterizations at similar reaction conditions. Hence, in the following, we continue to study the reduction of the Pt 2D surface oxide as in the 3/4 ML O surface phase. To this end, we employ the constant-potential method as described in the Computational Methods section. The advantage of the method is that it can properly "drain" or "fill" electrons according to the applied voltage so that it decouples the addition of H^+ and e^- and thus we can distinguish between an electrochemical proton−electron coupled-transfer step or a chemical H^+ addition step, which significantly helps determination of the Pt dissolution mechanism.

We simulate the reduction cycle first by adding four H atoms sequentially to one of PtO_4 units in the surface oxide, which results in $Pt(OH)_4$ hydroxide. The atomic structures of the reduced surface oxide with one−four added H atoms are shown in Figure 3a. The reaction free energies (ΔG's) of these reduction processes as a function of electrode potential are shown in Figure 3b. We assume the electrolyte has a pH = 1. All
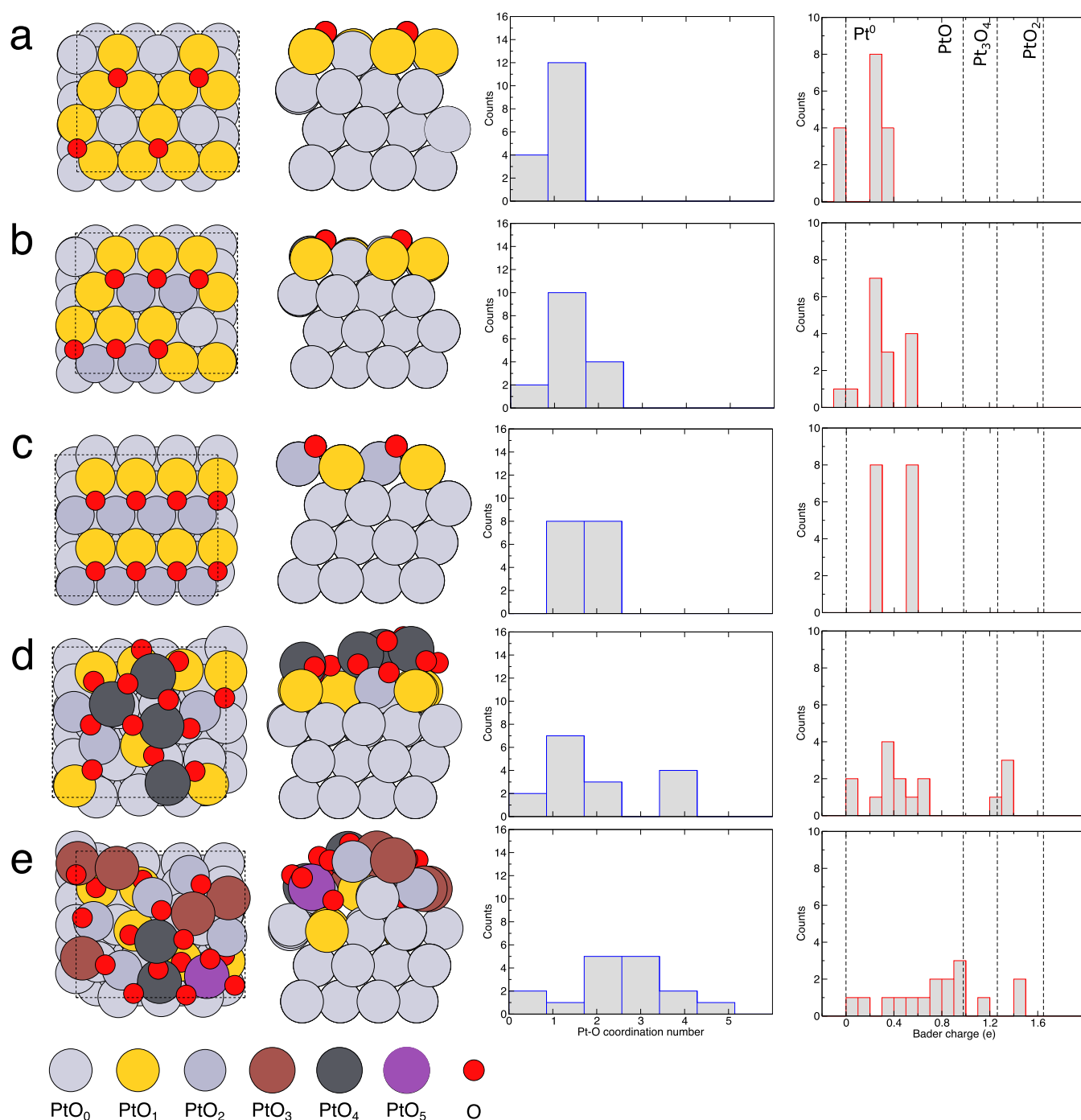
Figure 2. Optimized surface structures of oxidized Pt(111) surfaces with various O coverages. Along with the atomic structures, the corresponding histograms of Pt−O coordination number ($CN_{Pt−O}$) and Bader charges of surface Pt atoms are also shown. The O surface coverages are: (a) 1/4 ML O, (b) 3/8 ML, (c) 1/2 ML O, (d) 3/4 dML O, and (e) 1 ML O.

four ΔG's increase linearly with the electrode potential due to the reductive nature of these processes. The slopes of the ΔG's are in the range of 0.71−0.87e, indicating the amount of transferred electrons in these reactions. The first H addition becomes thermodynamically favorable when the applied potential drops below 1.17 V_{SHE}. The addition of the fourth H requires the lowest potential of 1.07 V_{SHE}. The oxidation state of the Pt ion decreases as more H atoms are added. As seen in Figure 3c. the Bader charge of the Pt ion drops from +1.3e to +1.15e after adding four H atoms, which means the oxidation state of the Pt ion drops from near $Pt^{2.7+}$ to somewhere between

$Pt^{2.7+}$ and Pt^{2+}. Structurally, the average Pt−O bond length elongates from 1.98 Å as in the PtO_4 to 2.03 Å after being reduced to $Pt(OH)_4$. The height of the center Pt atom rises about only 0.2 Å after reduction, signaling that no Pt dissolution has occurred so far.

We continue to study the further reduction of $Pt(OH)_4$. We first add one H atom to each O atom in the surface oxide to fully reduce the surface to Pt hydroxide. Starting from this structure, we further reduce the $Pt(OH)_4$ unit by successively adding four more H atoms to it. The resulting atomic structures after optimization are shown in Figure 4a. The corresponding
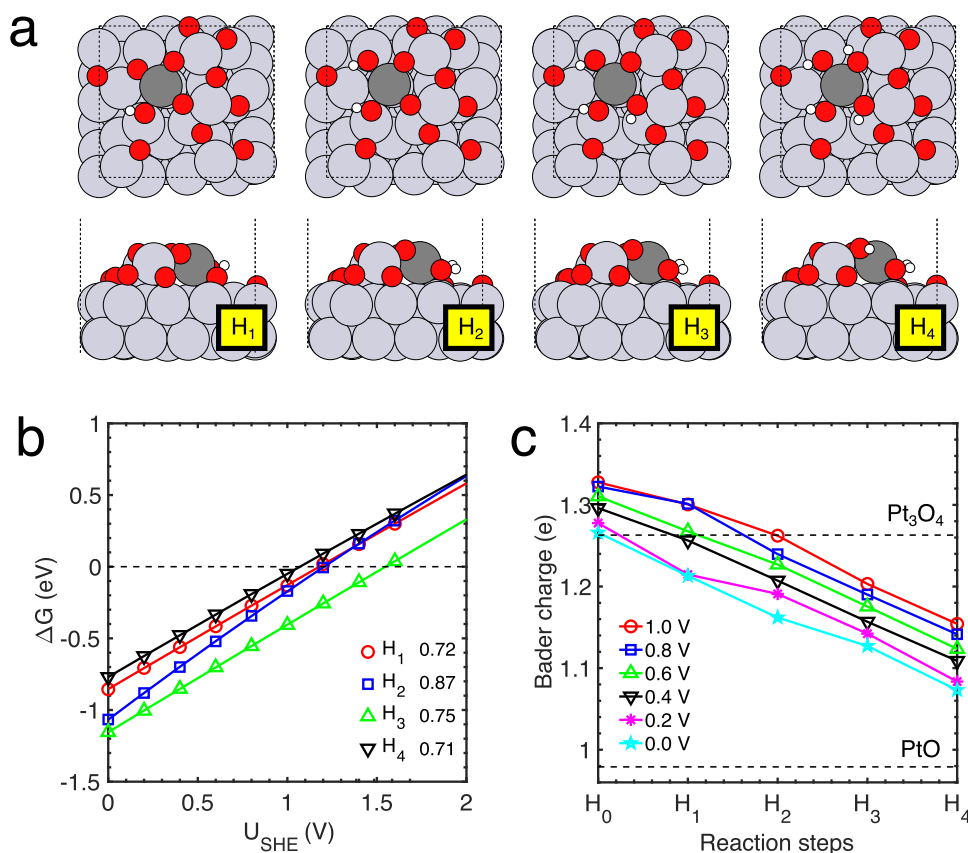
Figure 3. Reduction of a PtO_4 unit in the Pt surface oxide. (a) Top view and side view of atomic structures of progressively reduced PtO_4 having 1−4 H atoms added to it. (b) Potential-dependent reaction free energies of the PtO_4 reduction; the values indicate the number of electrons transferred in the reaction. (c) Bader charges of the Pt atom in PtO_4 along the reaction coordinate of the PtO_4 reduction at various applied potentials.

potential-dependent free energies of reaction and the Bader charges of the Pt ions are shown in Figure 4b,c. Addition of the fifth H has an onset potential of about 0.65 V_{SHE} at pH = 1. This reduction step leads to the formation of tightly bound H_2O to the Pt ion, as evidenced by the short Pt−O bond length of 2.06 Å. Comparatively, the H_2O adsorbed on the Pt(111) surface has a Pt−O bond length of 2.39 Å.[38] We calculate the desorption energy of H_2O from the Pt ion to be 1.3 eV at U = 0.65 V_{SHE}. The entropy of a water molecule in the bulk electrolyte is −0.67 eV,[2] which is not enough to compensate for the high desorption energy. The oxidation state of the central Pt atom stays roughly constant before and after the reduction, as shown in Figure 4c. The reduction is mainly on the Pt atom sharing the OH ligand with the centered Pt atom since it captures 0.16e and becomes Pt^0.

Similarly, the reduction of the second OH ligand also forms a tightly bound H_2O ligand with a Pt−O bond length of 2.06 Å. The reaction occurs at potentials below 0.8 V_{SHE} at pH = 1. The formed $Pt(OH)_2(H_2O)_2$ raises from the surface by 1.1 Å compared to the original height of the PtO_4 unit, signaling the beginning of Pt dissolution. The reduction of the third OH ligand leads to the complete dissolution of $Pt(OH)(H_2O)_3$. The process becomes thermodynamically favorable only at potentials of about 0.8 V_{SHE}. The dissolution of $Pt(OH)(H_2O)_3$ causes significant reconstruction to its two neighboring $Pt(OH)_4$. The square planar structures of the neighboring $Pt(OH)_4$ decompose to Pt with adsorbed OH due to ligand losses. Bader analysis shows that the oxidation states of the two neighboring Pt atoms change from Pt^{2+} to $Pt^{\delta+}$. The dissolved $Pt(OH)(H_2O)_3$ energetically prefers to be protonated to form $Pt(H_2O)_4$. This

step is a chemical step as indicated by the low slope (0.25e) of $\Delta G(U)$. The oxidation state of the central Pt atom is close to that of PtO, so we assign the dissolved Pt species as $[Pt(H_2O)_4]^{2+}$. The Pt−O bond length in $[Pt(H_2O)_4]^{2+}$ is calculated to be 2.03 Å, which is close to the experimental value of 2.02 Å.[39]

Pt dissolution during the cathodic scan is in competition with complete reduction to Pt metal. The atomic process of complete Pt reduction is shown in Figure 5a. This process combines OH reduction to H_2O and H_2O desorption. The reaction free energy of adding the fifth H atom in Figure 5b demonstrates that the process requires a low cathodic potential of about 0.2 V_{SHE} due to the strong interaction between H_2O ligand and the Pt ion. The reductive removal of the second OH ligand can occur at potentials as high as 1.1 V_{SHE}. This is due to a decrease in the oxidation state below Pt^{2+} after the first OH ligand loss, as shown in Figure 5c. The removal of the third OH ligand requires a low potential about 0.2 V_{SHE}, again because the ligand is part of a neighboring interacting $Pt(OH)_4$ unit. After the removal of the last OH ligand, the Pt ion is completely reduced to Pt metal, as shown in Figure 5c.

The reaction free energy of the Pt dissolution process during the cathodic cycle is plotted along the reaction coordinate at various applied potentials. As seen in Figure 6a, the reduction of PtO_4 to $Pt(OH)_4$ occurs spontaneously at U = 1.04 V_{SHE}. For $Pt(OH)_4$ to $[Pt(H_2O)_4]^{2+}$, the reaction free energies of all steps become spontaneous at U = 0.6 V_{SHE}, as shown in Figure 6b. On the other hand, the complete reduction of $Pt(OH)_4$ only becomes spontaneous at U = 0.18 V_{SHE}, as shown in Figure 6c. The onset potential gap between Pt dissolution and Pt complete
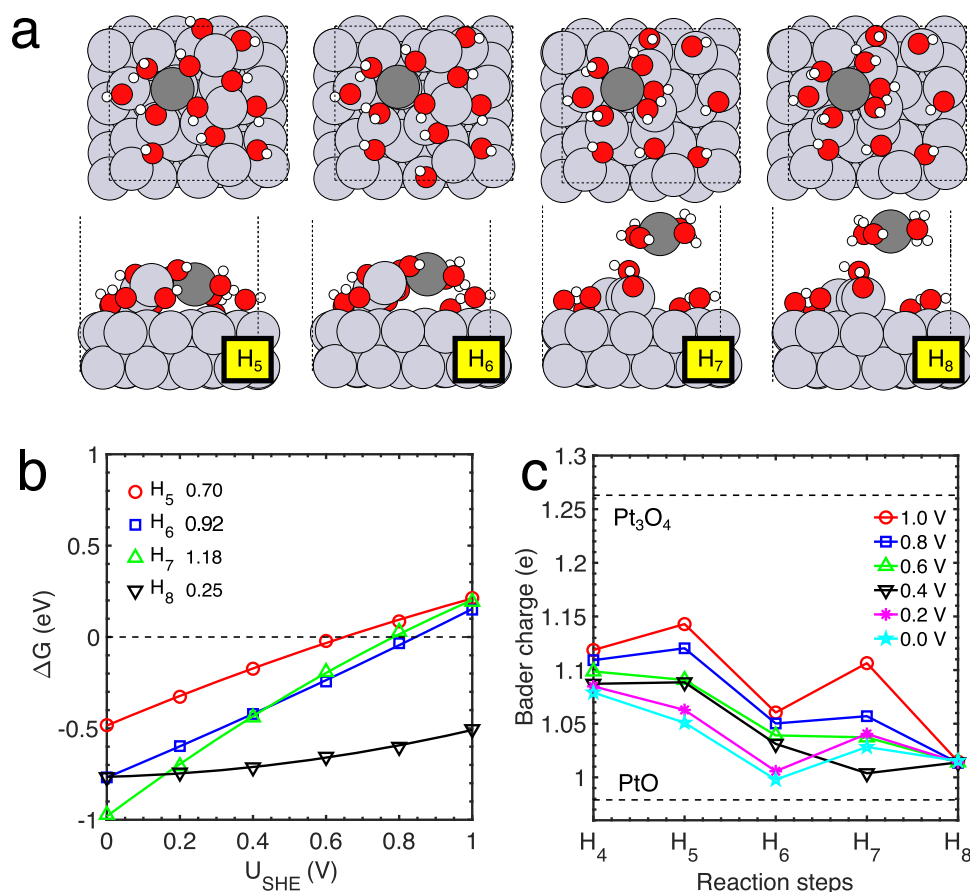
Figure 4. Reduction of $Pt(OH)_4$ unit in Pt surface oxide. (a) Top view and side view of atomic structures of progressively reduced $Pt(OH)_4$ having one−four H atoms added to it. (b) Potential-dependent reaction free energies of the $Pt(OH)_4$ reduction; the values indicate the number of electrons transferred in the reaction. (c) Bader charges of the Pt atom in $Pt(OH)_4$ along the reaction coordinate of the $Pt(OH)_4$ reduction at various applied potentials.

reduction could be used to explain the experimentally observed scan rate-dependent Pt dissolution[10,12] since a quick scan to low cathodic potentials would activate the complete reduction path that is competitive to the Pt dissolution path and hence leads to less Pt dissolution.

Mechanism of Pt Dissolution. Based on the results presented above, the reaction mechanism of Pt dissolution during potential cycling can be proposed. During the anodic scan, the Pt surface is gradually oxidized and undergoes a surface reconstruction to a 2D surface oxide at $U > 1.1\ V_{RHE}$. The 2D surface oxide consists of corner-sharing square planar PtO_4 motifs, which is similar to the atomic structure of bulk Pt_3O_4 oxide. The Pt ions in the 2D oxide also have an oxidation state similar to those in the bulk Pt_3O_4 oxide. During the cathodic scan, the surface oxide is reduced to Pt hydroxide consisting of $Pt(OH)_4$ units at $U \sim 1.0\ V_{RHE}$ at pH = 1. Pt hydroxide can be further reduced and dissolved in the form of $[Pt(H_2O)_4]^{2+}$. It is worth noting that not all Pt atoms in the surface oxide could dissolve during the reduction cycle because Pt dissolution causes the decomposition of the corner-sharing $Pt(OH)_4$ framework. Our simulations show that, along with the dissolution of one Pt atom, two connected Pt ions in the surface oxide are reduced to $Pt^{\delta+}$ due to the loss of ligands. It is expected that these Pt atoms can be readily reduced to Pt^0. For one dissolved atom, we find that approximately six electrons are transferred (by adding all transferred electrons in all eight H addition steps) during the reduction cycle. Based on the above information, we propose

that the Pt dissolution proceeds as follows during potential cycling

$$\text{anodic scan:}\quad 3Pt + 4H_2O \rightarrow Pt_3O_4^s + 8(H^+ + e^-) \quad (5)$$

$$\text{cathodic scan:}\quad Pt_3O_4^s + 8H^+ + 6e^-$$
$$\rightarrow [Pt(H_2O)_4]^{2+} + 2Pt \quad (6)$$
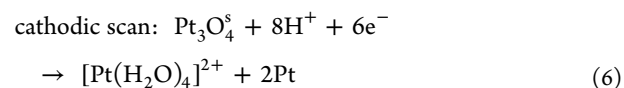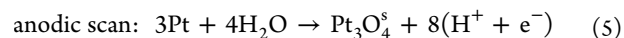
where $Pt_3O_4^s$ indicates the Pt_3O_4 surface oxide. In the experiment, minor anodic dissolution of Pt is also observed at potentials as low as $0.85\ V_{RHE}$.[14] In light of our simulation results, we propose the anodic Pt dissolution can be explained by the formation and dissolution of transiently formed Pt hydroxide, which can be written as

$$\text{anodic dissolution:}\quad Pt + 4H_2O$$
$$\rightarrow Pt(OH)_2 + 2H_2O + 2(H^+ + e^-)$$
$$\rightarrow [Pt(H_2O)_4]^{2+} + 2e^- \quad (7)$$
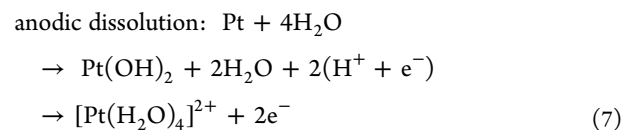
In this mechanism, Pt is first oxidized to Pt hydroxide, i.e., $Pt(OH)_2$. Then, the Pt hydroxide can be dissolved in the form of $[Pt(H_2O)_4]^{2+}$ via water adsorption and H^+ addition. We expect that the formation of $Pt(OH)_2$ and subsequent anodic dissolution would occur at defect sites on the Pt surface such as Pt ad-islands or step edges since the hydroxide is more likely to appear at these defect sites at low anodic potentials.
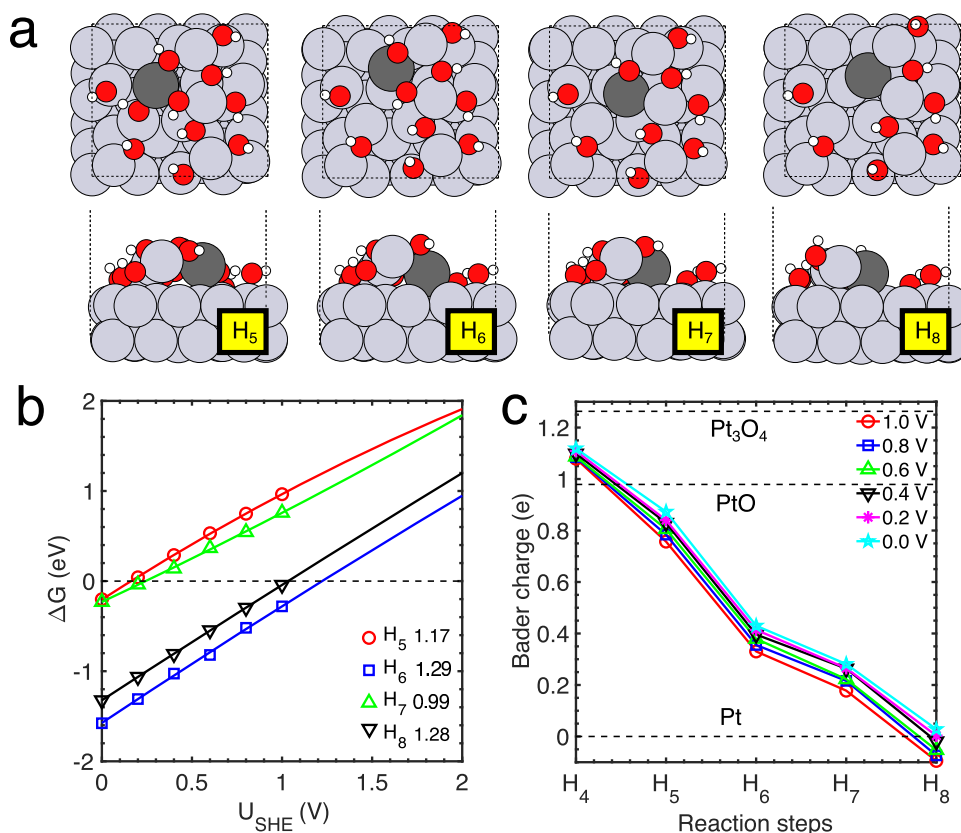
Figure 5. Complete reduction of $Pt(OH)_4$ unit in Pt surface oxide. (a) Top view and side view of atomic structures of progressive removal of the four OH ligands. (b) Potential-dependent reaction free energies of the complete $Pt(OH)_4$ reduction; the values indicate the number of electrons transferred in the reaction. (c) Bader charges of the Pt atom in $Pt(OH)_4$ along the reaction coordinate of the complete $Pt(OH)_4$ reduction at various applied potentials.
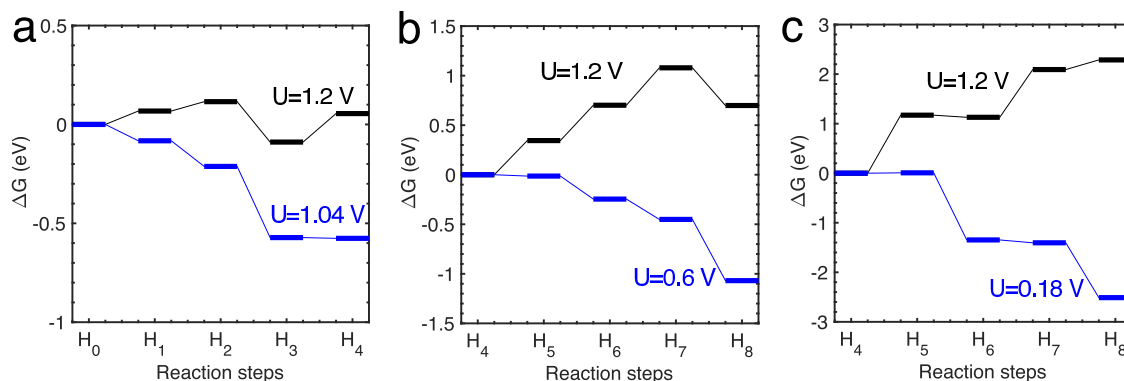
Figure 6. Free-energy landscapes of (a) PtO_4 reduction to $Pt(OH)_4$, (b) $Pt(OH)_4$ reduction to $Pt(H_2O)_4{}^{2+}$, and (c) complete reduction of $Pt(OH)_4$ to Pt metal at various applied potentials.

The presence of Cl^- ions in the electrolyte has been demonstrated to significantly enhance both anodic and cathodic Pt dissolution.[40,41] Based on the mechanism discussed above, we propose the enhanced anodic Pt dissolution is due to Cl^- ions interfering with further oxidation of the surface Pt hydroxide, thus leading to the formation of highly soluble $PtCl_4{}^{2-}$. This reaction can be written as $Pt(OH)_2 + 4Cl^- + 2H^+ \rightarrow PtCl_4{}^{2-} + 2H_2O$. Similarly, for the cathodic Pt dissolution, Cl^- ions could exchange with the H_2O ligands in $[Pt(H_2O)_4]^{2+}$ via the reaction: $[Pt(H_2O)_4]^{2+} + 4Cl^- \rightarrow PtCl_4{}^{2-} + 4H_2O$. Thus, due to the increased solubility, the redeposition of the Pt ions would be reduced.

In the mathematical modeling of Pt dissolution kinetics under potentiostatic conditions, a mechanism combining Pt anodic dissolution and chemical dissolution of the formed Pt oxides has been described.[42,43] This mechanism predicts a lower Pt dissolution rate compared to that under potential cycling conditions, which indicates that a fundamentally different mechanism governs the latter.[43,44] Kinetic models considering potential cycling have also been developed and show good predictive capabilities for Pt particle radius distribution (PSD) evolution and electrochemically active surface area (ECSA) loss.[44] However, these models rely on parameters taken from empirical studies or data fitting. Our work provides atomistic insights into the Pt oxidation/dissolution process and especially

cathodic Pt dissolution that is lacking in the reaction models adopted in previous kinetic studies. Hence, we expect that implementing our proposed Pt dissolution mechanisms from eqs 5, 6, and 7 into the kinetic models could lead to more realistic reaction models.

CONCLUSIONS

We employed DFT calculations to investigate the atomic-scale mechanism of Pt dissolution during potential cycling. We discover that the Pt(111) surface is first oxidized to form a 2D surface oxide consisting of square planar PtO_4 units at $U > 1.1$ V_{RHE} during the anodic scan. The surface oxide can be reduced during the following cathodic scan and dissolved as [Pt-$(H_2O)_4]^{2+}$. The free-energy landscape of the reduction and dissolution process suggests the Pt dissolution becomes spontaneous at potentials below 0.6 V_{SHE} at pH = 1. In contrast, the complete reduction of Pt becomes spontaneous at lower cathodic potentials at 0.18 V_{SHE} at pH = 1. Moreover, we find that a dissolved Pt species can cause nearby Pt atoms in the surface oxide to be readily reduced to Pt metal due to losses of ligands. Our study provides atomic-scale fundamental understandings on the Pt dissolution process under potential cycling. Based on these atomic-level insights, we believe mitigation strategies of Pt dissolution can be designed accordingly in the future.

ASSOCIATED CONTENT

ⓈⒾ Supporting Information

The Supporting Information is available free of charge at https://pubs.acs.org/doi/10.1021/acscatal.1c02366.

> Convergence properties of the genetic algorithm optimizations, surface structures of Pt surface oxides that do not show up in the surface Pourbaix diagram, and atomic models of the Pt bulk oxides (PDF)

AUTHOR INFORMATION

Corresponding Authors

Zhiyao Duan − *State Key Laboratory of Solidification Processing, School of Materials Science and Engineering, Northwestern Polytechnical University, Xi'an 710072, P. R. China*; Email: zhiyao.duan@nwpu.edu.cn

Graeme Henkelman − *Department of Chemistry and the Oden Institute for Computational Engineering and Sciences, The University of Texas at Austin, Austin, Texas 78712-0165, United States*; ⓞ orcid.org/0000-0002-0336-7153; Email: henkelman@utexas.edu.

Complete contact information is available at:
https://pubs.acs.org/10.1021/acscatal.1c02366

Notes

The authors declare no competing financial interest.

ACKNOWLEDGMENTS

REFERENCES

(1) Kodama, K.; Nagai, T.; Kuwaki, A.; Jinnouchi, R.; Morimoto, Y. Challenges in applying highly active Pt-based nanostructured catalysts for oxygen reduction reactions to fuel cell vehicles. *Nat. Nanotechnol.* **2021**, *16*, 140−147.

(2) Nørskov, J. K.; Rossmeisl, J.; Logadottir, A.; Lindqvist, L.; Kitchin, J. R.; Bligaard, T.; Jónsson, H. Origin of the Overpotential for Oxygen Reduction at a Fuel-Cell Cathode. *J. Phys. Chem. B* **2004**, *108*, 17886−17892.

(3) Shao-Horn, Y.; Sheng, W. C.; Chen, S.; Ferreira, P. J.; Holby, E. F.; Morgan, D. Instability of Supported Platinum Nanoparticles in Low-Temperature Fuel Cells. *Top. Catal.* **2007**, *46*, 285−305.

(4) de Bruijn, F. A.; Dam, V. A. T.; Janssen, G. J. M. Review: Durability and Degradation Issues of PEM Fuel Cell Components. *Fuel Cells* **2008**, *8*, 3−22.

(5) Fantauzzi, D.; Mueller, J. E.; Sabo, L.; van Duin, A. C. T.; Jacob, T. Surface Buckling and Subsurface Oxygen: Atomistic Insights into the Surface Oxidation of Pt(111). *ChemPhysChem* **2015**, *16*, 2797−2802.

(6) Eslamibidgoli, M. J.; Eikerling, M. H. Atomistic Mechanism of Pt Extraction at Oxidized Surfaces: Insights from DFT. *Electrocatalysis* **2016**, *7*, 345−354.

(7) Fuchs, T.; Drnec, J.; Calle-Vallejo, F.; Stubb, N.; Sandbeck, D. J. S.; Ruge, M.; Cherevko, S.; Harrington, D. A.; Magnussen, O. M. Structure dependency of the atomic-scale mechanisms of platinum electro-oxidation and dissolution. *Nat. Catal.* **2020**, *3*, 754−761.

(8) Kirchhoff, B.; Braunwarth, L.; Jung, C.; Jónsson, H.; Fantauzzi, D.; Jacob, T. Simulations of the Oxidation and Degradation of Platinum Electrocatalysts. *Small* **2020**, *16*, No. 1905159.

(9) Topalov, A. A.; Katsounaros, I.; Auinger, M.; Cherevko, S.; Meier, J. C.; Klemm, S. O.; Mayrhofer, K. J. J. Dissolution of Platinum: Limits for the Deployment of Electrochemical Energy Conversion? *Angew. Chem., Int. Ed.* **2012**, *51*, 12613−12615.

(10) Topalov, A. A.; Cherevko, S.; Zeradjanin, A. R.; Meier, J. C.; Katsounaros, I.; Mayrhofer, K. J. J. Towards a comprehensive understanding of platinum dissolution in acidic media. *Chem. Sci.* **2014**, *5*, 631−638.

(11) Lopes, P. P.; Strmcnik, D.; Tripkovic, D.; Connell, J. G.; Stamenkovic, V.; Markovic, N. M. Relationships between Atomic Level Surface Structure and Stability/Activity of Platinum Surface Atoms in Aqueous Environments. *ACS Catal.* **2016**, *6*, 2536−2544.

(12) Lopes, P. P.; Tripkovic, D.; Martins, P. F.; Strmcnik, D.; Ticianelli, E. A.; Stamenkovic, V. R.; Markovic, N. M. Dynamics of electrochemical Pt dissolution at atomic and molecular levels. *J. Electroanal. Chem.* **2018**, *819*, 123−129.

(13) Myers, D. J.; Wang, X.; Smith, M. C.; More, K. L. Potentiostatic and Potential Cycling Dissolution of Polycrystalline Platinum and Platinum Nano-Particle Fuel Cell Catalysts. *J. Electrochem. Soc.* **2018**, *165*, F3178−F3190.

(14) Cherevko, S.; Keeley, G. P.; Geiger, S.; Zeradjanin, A. R.; Hodnik, N.; Kulyk, N.; Mayrhofer, K. J. J. Dissolution of Platinum in the Operational Range of Fuel Cells. *ChemElectroChem* **2015**, *2*, 1471−1478.

(15) Sandbeck, D. J. S.; Brummel, O.; Mayrhofer, K. J. J.; Libuda, J.; Katsounaros, I.; Cherevko, S. Dissolution of Platinum Single Crystals in Acidic Medium. *ChemPhysChem* **2019**, *20*, 2997−3003.

(16) Kresse, G.; Hafner, J. Ab Initio Molecular Dynamics for Liquid Metals. *Phys. Rev. B* **1993**, *47*, 558.

(17) Kresse, G.; Furthmüller, J. Efficiency of Ab-Initio Total Energy Calculations for Metals and Semiconductors Using a Plane-Wave Basis Set. *Comput. Mater. Sci.* **1996**, *6*, 15−50.

(18) Kresse, G.; Furthmüller, J. Efficient Iterative Schemes for Ab Initio Total-Energy Calculations Using a Plane-Wave Basis Set. *Phys. Rev. B* **1996**, *54*, 11169.

(19) Perdew, J. P.; Burke, K.; Ernzerhof, M. Generalized Gradient Approximation Made Simple. *Phys. Rev. Lett.* **1996**, *77*, 3865−3868.

(20) Blöchl, P. E. Projector augmented-wave method. *Phys. Rev. B* **1994**, *50*, 17953−17979.

(21) Monkhorst, H. J.; Pack, J. D. Special Points for Brillouin-Zone Integrations. *Phys. Rev. B* **1976**, *13*, 5188−5192.

(22) Henkelman, G.; Arnaldsson, A.; Jónsson, H. A fast and robust algorithm for Bader decomposition of charge density. *Comput. Mater. Sci.* **2006**, *36*, 354−360.

(23) Tang, W.; Sanville, E.; Henkelman, G. A grid-based Bader analysis algorithm without lattice bias. *J. Phys. Condens. Matter* **2009**, *21*, No. 084204.

(24) Vilhelmsen, L. B.; Hammer, B. A genetic algorithm for first principles global structure optimization of supported nano structures. *J. Chem. Phys.* **2014**, *141*, No. 044711.

(25) Van den Bossche, M.; Skúlason, E.; Rose-Petruck, C.; Jónsson, H. Assessment of Constant-Potential Implicit Solvation Calculations of Electrochemical Energy Barriers for H2 Evolution on Pt. *J. Phys. Chem. C* **2019**, *123*, 4116−4124.

(26) Duan, Z.; Xiao, P. Simulation of Potential-Dependent Activation Energies in Electrocatalysis: Mechanism of O−O Bond Formation on RuO2. *J. Phys. Chem. C* **2021**, *125*, 15243−15250.

(27) Hansen, H. A.; Rossmeisl, J.; Nørskov, J. K. Surface Pourbaix Diagrams and Oxygen Reduction Activity of Pt, Ag and Ni(111) Surfaces Studied by DFT. *Phys. Chem. Chem. Phys.* **2008**, *10*, 3722−3730.

(28) Ruge, M.; Drnec, J.; Rahn, B.; Reikowski, F.; Harrington, D. A.; Carlà, F.; Felici, R.; Stettner, J.; Magnussen, O. M. Electrochemical Oxidation of Smooth and Nanoscale Rough Pt(111): An In Situ Surface X-ray Scattering Study. *J. Electrochem. Soc.* **2017**, *164*, H608−H614.

(29) Drnec, J.; Ruge, M.; Reikowski, F.; Rahn, B.; Carlá, F.; Felici, R.; Stettner, J.; Magnussen, O. M.; Harrington, D. A. Initial stages of Pt(111) electrooxidation: dynamic and structural studies by surface X-ray diffraction. *Electrochim. Acta* **2017**, *224*, 220−227.

(30) Gómez-Marín, A. M.; Feliu, J. M. Oxide growth dynamics at Pt(111) in absence of specific adsorption: A mechanistic study. *Electrochim. Acta* **2013**, *104*, 367−377.

(31) Gómez-Marín, A. M.; Clavilier, J.; Feliu, J. M. Sequential Pt(111) oxide formation in perchloric acid: An electrochemical study of surface species inter-conversion. *J. Electroanal. Chem.* **2013**, *688*, 360−370.

(32) Zhu, J.; Hu, S.; Zeng, Z.; Li, W.-X. First-principles investigation of electrochemical dissolution of Pt nanoparticles and kinetic simulation. *J. Chem. Phys.* **2019**, *151*, No. 234711.

(33) Ehelebe, K.; Knöppel, J.; Bierling, M.; Mayerhöfer, B.; Böhm, T.; Kulyk, N.; Thiele, S.; Mayrhofer, K. J. J.; Cherevko, S. Platinum Dissolution in Realistic Fuel Cell Catalyst Layers. *Angew. Chem., Int. Ed.* **2021**, *60*, 8882−8888.

(34) Kaneko, T.; Samjeské, G.; Nagamatsu, S.-i.; Higashi, K.; Sekizawa, O.; Takao, S.; Yamamoto, T.; Zhao, X.; Sakata, T.; Uruga, T.; Iwasawa, Y. Key Structural Kinetics for Carbon Effects on the Performance and Durability of Pt/Carbon Cathode Catalysts in Polymer Electrolyte Fuel Cells Characterized by In Situ Time-Resolved X-ray Absorption Fine Structure. *J. Phys. Chem. C* **2016**, *120*, 24250−24264.

(35) Takagi, Y.; Wang, H.; Uemura, Y.; Nakamura, T.; Yu, L.; Sekizawa, O.; Uruga, T.; Tada, M.; Samjeské, G.; Iwasawa, Y.; Yokoyama, T. In situ study of oxidation states of platinum nanoparticles on a polymer electrolyte fuel cell electrode by near ambient pressure hard X-ray photoelectron spectroscopy. *Phys. Chem. Chem. Phys.* **2017**, *19*, 6013−6021.

(36) Imai, H.; Izumi, K.; Matsumoto, M.; Kubo, Y.; Kato, K.; Imai, Y. In Situ and Real-Time Monitoring of Oxide Growth in a Few Monolayers at Surfaces of Platinum Nanoparticles in Aqueous Media. *J. Am. Chem. Soc.* **2009**, *131*, 6293−6300.

(37) Mom, R.; Frevel, L.; Velasco-Vélez, J.-J.; Plodinec, M.; Knop-Gericke, A.; Schlögl, R. The Oxidation of Platinum under Wet Conditions Observed by Electrochemical X-ray Photoelectron Spectroscopy. *J. Am. Chem. Soc.* **2019**, *141*, 6537−6544.

(38) Ungerer, M. J.; Santos-Carballal, D.; Cadi-Essadek, A.; van Sittert, C. G. C. E.; de Leeuw, N. H. Interaction of H2O with the Platinum Pt (001), (011), and (111) Surfaces: A Density Functional Theory Study with Long-Range Dispersion Corrections. *J. Phys. Chem. C* **2019**, *123*, 27465−27476.

(39) Ayala, R.; Marcos, E. S.; Díaz-Moreno, S.; Solé, V. A.; Muñoz-Páez, A. Geometry and Hydration Structure of Pt(II) Square Planar Complexes [Pt(H2O)4]2+ and [PtCl4]2- as Studied by X-ray Absorption Spectroscopies and Quantum-Mechanical Computations. *J. Phys. Chem. B* **2001**, *105*, 7588−7593.

(40) Pavlišič, A.; Jovanovič, P.; Šelih, V. S.; Šala, M.; Hodnik, N.; Hočevar, S.; Gaberšček, M. The influence of chloride impurities on Pt/C fuel cell catalyst corrosion. *Chem. Commun.* **2014**, *50*, 3732−3734.

(41) Wang, Z.; Tada, E.; Nishikata, A. In Situ Analysis of Chloride Effect on Platinum Dissolution by a Channel-Flow Multi-Electrode System. *J. Electrochem. Soc.* **2014**, *161*, F845−F849.

(42) Darling, R. M.; Meyers, J. P. Kinetic Model of Platinum Dissolution in PEMFCs. *J. Electrochem. Soc.* **2003**, *150*, A1523.

(43) Rinaldo, S. G.; Stumper, J.; Eikerling, M. Physical Theory of Platinum Nanoparticle Dissolution in Polymer Electrolyte Fuel Cells. *J. Phys. Chem. C* **2010**, *114*, 5773−5785.

(44) Rinaldo, S. G.; Lee, W.; Stumper, J.; Eikerling, M. Model- and Theory-Based Evaluation of Pt Dissolution for Supported Pt Nanoparticle Distributions under Potential Cycling. *Electrochem. Solid-State Lett.* **2011**, *14*, B47.